Proceedings of 2021 IEEE
International Conference on Mechatronics and Automation
August 8 - 11, Takamatsu, Japan

Study on Hydrodynamic Characteristics and Dynamics Model of Underwater Spherical Robot

Ao Li[1], Shuxiang Guo[1,2], Liwei Shi[1], Xihuan Hou[1], Zan Li[1], Debin Xia[1]*

1 Key Laboratory of Convergence Medical Engineering System and Healthcare Technology, the Ministry of Industry and Information Technology, School of Life Science, Beijing Institute of Technology, No.5, Zhongguancun South Street, Haidian District, Beijing 100081, China

2 Faculty of Engineering, Kagawa University, 2217-20 Hayashi-cho, Takamatsu, Kagawa, Japan

{ liao & guoshuxiang & shiliwei } @bit.edu.cn;

* Corresponding author

***Abstract* - In order to simplify parameter adjustment process of the AUV controller in the pool experiments, many researchers established the robot dynamics model and pre-adjusted the parameters in the simulation. This paper mainly studied the characteristics of underwater spherical robot hydrodynamic model and the verification of the model through experiments. First, we obtained the hydrodynamic force acting of the robot in different fluid environments through Computational Fluid Dynamic method. Then, the hydrodynamic coefficients of the dynamic model were calculated by the regression of the above force data. Finally, these hydrodynamic coefficients obtained from the above simulation were verified by pool experiments. The experimental results showed that these coefficients obtained by this method was well fitted with the experimental data and may be used as a reference for the hydrodynamic model. In addition, the nonlinear characteristics of hydrodynamic coefficients under different disturbances were also studied. This will provide further reference for model identification and control in complex underwater environment.**

Index Terms* - *underwater spherical robot, Computational Fluid Dynamic, hydrodynamic modeling, robot motion.

I. INTRODUCTION

With the frequent and deep utilization of water environment (such as ocean) resources, various types of underwater vehicles have been developed [1]. Among them, underwater spherical robot has been extensively studied because of its stable structure, flexible movement, and adaptability to underwater exploration [2]. These advantages make underwater spherical robot play an important role in terrain and resource detection [3], cooperative operation [4] and other fields [5]. However, under the reality of complex hydrodynamic environment conditions, the current movement performance of the robot cannot perfectly realize the expected exploration target [6].

Parameter testing and adjustment of motion controller is one of the obstacles to the performance improvement of underwater robot [7]. Due to the limitation of energy and surrounding environment, it is challenging, time-consuming and resource-consuming to adjust parameters of underwater robot in actual pool experiment [8]. Therefore, it is an efficient way to first determine the approximate parameters during simulation and then further adjust these parameters in the underwater experiment of the robot [9]. Based on the above analysis, a dynamic model with accurate hydrodynamic coefficients is essential.

The fluid around the moving underwater robot is relatively strong and complex, which leads to the highly nonlinear and coupling of the kinematics and dynamics models of the AUV[10]. Therefore, in general, it is difficult to model the robot dynamics model with accurate hydrodynamic coefficients. However, hydrodynamics coefficients of the robot dynamics model are very important to accurately simulate the dynamic performance and the further control of the underwater robot[11]. Based on this, we focus on the acquisition of hydrodynamic coefficients in the dynamic modeling of the underwater robot.

The acquisition methods of hydrodynamic coefficients mainly include test-based methods, predictive methods, and computational fluid dynamics (CFD) methods. Test-based methods is based on towing-tank model tests. The disadvantage of this method is that the need for the vehicle model itself and corresponding laboratory facilities can reduce availability and increase the cost of testing [12]. The predictive methods get the hydrodynamic coefficients through theoretical analysis [13]. This method can be applied to typical streamlined cylindrical underwater vehicle [14], but the modeling error is usually large for complex underwater vehicle [15]. For example, for underwater spherical robots, the distribution and importance of each hydrodynamic coefficient will be somewhat different [16]. Computational fluid dynamics (CFD) method has been widely used in the simulation of the flow field generated by underwater vehicle movement [17], and can also be used in the calculation of hydrodynamic model [18]. This method can obtain all the corresponding hydrodynamic coefficients more accurately, and build the dynamics model of the robot based on these coefficients [19].

In this paper, the modeling of underwater spherical robot based on CFD simulation was calculated. The effect of damping force coefficients caused by water flow on robot dynamics was studied. The purpose was to predict the coefficients that related to hydrodynamics in the robot dynamics model, so as to provide reliable guidance for the control of robot. Based on this dynamic model, we generated the process of robot movement through simulation under certain conditions. Then, experiments were carried out on underwater spherical robots to obtain the robot's movement process in the pool under the same conditions. The comparison of the robot movement based on simulation and experiment verified the effectiveness of the modeling method.

978-1-6654-4098-1/21/$31.00 ©2021 IEEE

II. Dynamics Modeling

A. Dynamics Equation of the Spherical Robot

Our study was mainly based on the Amphibious Spherical Robot V (ASR-V), whose structure was shown in Fig. 1(a). The robot consists of an approximately hemispherical body and four thrusters that can be arranged in an H shape (as shown in Fig. 1(b)), which enables the robot to move forward and turn flexibly on a horizontal plane. In addition, the related fine structures in Fig. 1(a) were simplified in Fig. 1(b) to facilitate the simulation of Computational Fluid Dynamic. The robot is designed to explore underwater environments such as shallow seas, lakes and rivers.

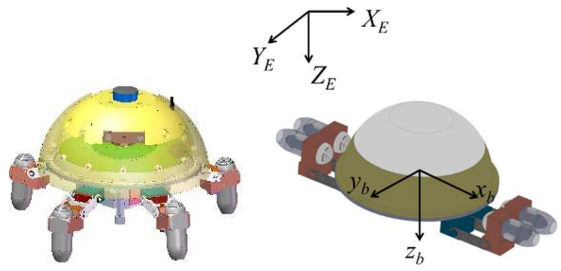

（a） （b）

Fig. 1 The model structure of the ASR. (a) The Structure of ASR-V robot. (b) Robot with H-shaped arrangement of thrusters. The model has been partially simplified for better hydrodynamic calculations.

The radius of ASR-V shell is 0.15 meters, and the total weight of this robot is 6.7 kilograms. To describe the motion of ASR-V, two coordinate systems are defined, as shown in Fig. 1(b). The first is the inertial coordinate system $O_E - X_E, Y_E, Z_E$ with the origin fixed on the earth surface. The second is the reference coordinate system $O_b - x_b, y_b, z_b$ fixed on the robot body, and the origin O_b is fixed on the center of the robot. When the robot moves, its position and attitude can be represented by the vectors $\boldsymbol{\eta} = [x, y, z, \phi, \theta, \psi]^T$. Its velocity and angular velocity can be expressed by the vector $\mathbf{v} = [u, v, w, p, q, r]^T$. Finally, the forces and torques acting on the robot can be expressed by the vectors $\boldsymbol{\tau} = [X, Y, Z, K, M, N]^T$. The dynamics model of the robot can be described as [20]:

$$\boldsymbol{\tau} = \mathbf{M}\dot{\mathbf{v}} + \mathbf{C}(\mathbf{v})\mathbf{v} + \mathbf{D}(\mathbf{v}) + \mathbf{g}(\boldsymbol{\eta}), \tag{1}$$

where,

$$\mathbf{M} = \mathbf{M_{RB}} + \mathbf{M_A} = diag\{m, m, m, I_x, I_y, I_z\} - diag\{X_{\dot{u}}, Y_{\dot{v}}, Z_{\dot{w}}, K_{\dot{p}}, M_{\dot{q}}, N_{\dot{r}}\} \tag{2}$$

$$\mathbf{C}(\mathbf{v}) = \mathbf{C_{RB}}(\mathbf{v}) + \mathbf{C_A}(\mathbf{v}) \tag{3}$$

$$\mathbf{D}(\mathbf{v}) = \mathbf{D_1}(\mathbf{v}) + \boldsymbol{D_2}(\mathbf{v})\mathbf{v} \tag{4}$$

$\mathbf{g}(\boldsymbol{\eta})$ is the restorative force. For ASR, the center of mass is located below the center of buoyancy, so the restorative force remains vertical. $\mathbf{M_{RB}}$ is the rigid body inertia matrix, $\mathbf{C_{RB}}$ is the rigid body Coriolis-centripetal force matrix, $\mathbf{M_A}$ is the additional mass force matrix, and $\mathbf{C_A}$ is the additional Coriolis-centripetal force matrix. $\mathbf{D}(\mathbf{v})$ is the hydrodynamic damping of the ASR, and this dynamic term is the main concern in our subsequent studies. At present, the basic model for the hydrodynamic damping coefficients are mostly based on the following three assumptions [21]:

1) The model neglects linear and angular coupled terms.

2) The model assumes that the robot is top-bottom and port starboard symmetric.

3) The model neglects any damping terms greater than second order.

However, hydrodynamic damping is coupled and highly nonlinear, especially for complex shape underwater robots. Therefore, we analyze the variation characteristics of the hydrodynamic damping coefficients under different flow disturbance.

B. Computational Fluid Dynamic

The model of the robot under the CFD software ANSYS CFX is shown in Fig. 2. The computing domain is 3.5m in length, 3.5m in width and 3.1m in height, and the robot is set in the center of the computing domain. In addition, there is a rotation domain with a diameter of 1.1m and a height of 0.65m, which is used to simulate the hydrodynamic performance during the yaw motion of the robot. Fig. 3(a) shows the meshing of the computational domain in CFD, which contains 497,784 nodes and 2,630,860 elements. The meshing of the robot surface and its surrounding computing domain is shown in Fig. 3(b).

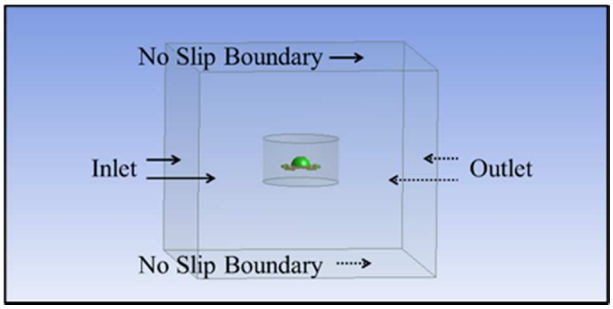

Fig. 2 The CFD model of the robot.

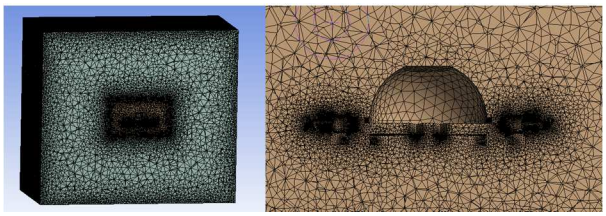

(a) (b)

Fig. 3 The meshing of the simulation area. (a) The meshing of the computational domain in CFD. (b) The meshing of the robot surface and its surrounding computing domain.

The basis of CFD is the governing equations of fluid dynamics -- continuity, momentum conservation and energy conservation [22]. According to the Reynolds number calculation principle, when the robot moves at a velocity of about 0.1m/s, the Reynolds number is about 30,000. Therefore, a shear stress transport (SST) turbulence model was selected as the turbulence model in this paper. It has good stability and has

been widely used in the field of turbulence calculation. The SST model is based on the k-w model. Fig. 2 marks the boundary conditions of the computing domain, where the inlet is the entry of the computing domain and the outlet is the exit of the computing domain. The boundary conditions are set as follows: the inlet boundary is the inflow port of the flow field, and the velocity of the entire flow field is changed by the input velocity of the inlet boundary; The outlet boundary is the fluid flow outlet and is set as the constant pressure boundary. The others is set as no slip boundary. In the simulation, the robot remains stationary and the fluid flows from the inlet to the outlet. The principle of relative motion can be used to understand the motion of underwater robot.

The grid independence of this computing domain has been verified, as shown in Fig. 4. The diamond point represents the grid scale selected for calculating the data used in this article. The selection of this scale not only ensures the accuracy of the computing results, but also ensures the high utilization rate of the computing resources.

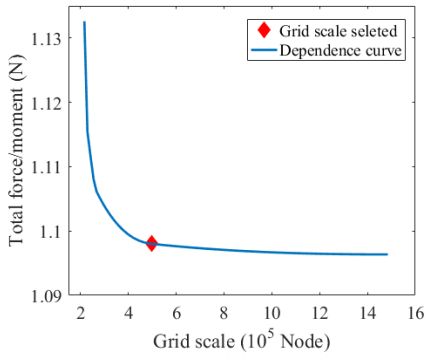

Fig. 4 The grid independence validation of the computing domain.

III. Model Identification And Validation

The CFD modeling and hydrodynamic analysis of underwater spherical robot are the preliminary analysis to determine the influence of each hydrodynamic coefficient. In this section, we will discuss the dynamic models of the robot in surge motion and yaw motion, focusing on the identification of the relevant hydrodynamic damping coefficients.

A. Model identification of surge motion

TABLE I
THE COMPUTING RESULTS OF ASR HYDRODYNAMIC DAMPING AT DIFFERENT SURGE VELOCITY

surge velocity (m/s)	surge damping (N)	surge velocity (m/s)	surge damping (N)
0.00	-0.00020	0.20	0.44516
0.02	0.00544	0.22	0.53802
0.04	0.01928	0.24	0.63986
0.06	0.04186	0.26	0.75051
0.08	0.07293	0.28	0.87046
0.10	0.11278	0.30	0.99881
0.12	0.16119	0.32	1.13579
0.14	0.21879	0.34	1.28167
0.16	0.28528	0.36	1.43652
0.18	0.36097	0.38	1.60013

surge motion is the most common mode of robot underwater movement. Based on this, we designed a set of hydrodynamic simulations at different surge velocity without disturbances, as shown in Table 1.

The table lists the computing results of hydrodynamic damping acting on the ASR at different surge velocity. In the table, the surge damping force was calculated by integrating the surface pressure of the robot along the axis. The hydrodynamic damping coefficients of surge motion can be obtained by regression analysis of the computing results in Table 1.

The damping coefficients are often assumed to be linear based on the assumption of small disturbances. Through model identification, the relationship between the hydrodynamic damping of the robot and the surge velocity without disturbances can be obtained as follows:

$$F_X = -0.0155u - 11.0365u^2 \tag{5}$$

We assumed that the damping coefficients of the robot only contain the velocity and quadratic velocity terms. From the identification formula and the regression analysis, we concluded that the damping of surge motion was linearly related mainly to the quadratic velocity, but less to the first order of velocity.

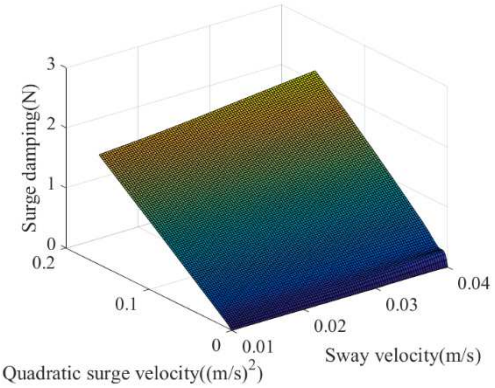

Fig. 5 The relationship curve between the damping force of surge motion and the quadratic surge velocity and the disturbance velocity (sway velocity).

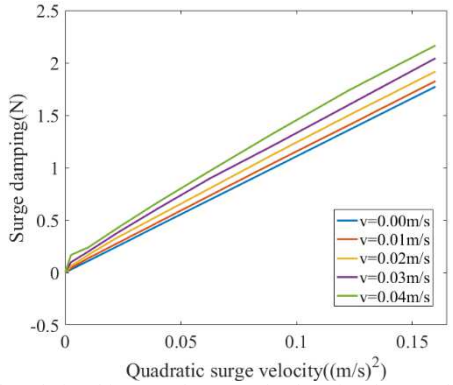

Fig. 6 The relationship curve between the damping force and the quadratic velocity of the robot under different sway velocity disturbance.

Furthermore, we designed the hydrodynamic simulation when the velocity disturbance existed in the sway direction of the robot, as shown in Fig. 5. The figure described the relation

between the damping force of surge motion and the quadratic surge velocity and the disturbance velocity (sway velocity). We concluded that the surge damping force was related to both velocities mentioned above, but it was not completely linear. In order to further analyze the influence of disturbance on the damping coefficients, Fig. 5 was decomposed according to the disturbance velocity to obtain Fig. 6.

Fig. 5 showed the relationship curve between the damping force and the quadratic velocity of the robot under different sway velocity disturbance. The damping coefficients were constant with constant sway velocity disturbances.

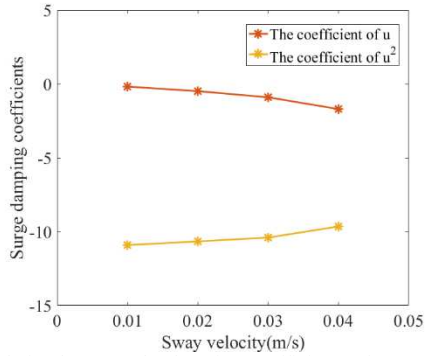

Fig. 7 The relation between the damping coefficients of surge motion and the disturbance velocity in sway direction.

As shown in Fig. 7, the relationship between the damping coefficients and the disturbance velocity was obtained through regression analysis. It was shown that the change of the damping coefficients with the increase of the disturbance velocity was nonlinear.

B. Model identification of yaw motion

TABLE I
THE COMPUTING RESULTS OF ASR HYDRODYNAMIC DAMPING AT DIFFERENT YAW VELOCITY

sway angular velocity (m/s)	sway damping (N)	sway angular velocity (m/s)	sway damping (N)
0.0000	-0.00006	0.1163	-0.00180
0.0116	-0.00015	0.1400	-0.00240
0.0232	-0.00016	0.1570	-0.00287
0.0349	-0.00023	0.1745	-0.00343
0.0465	-0.00036	0.1919	-0.00402
0.0582	-0.00053	0.2094	-0.00467
0.0698	-0.00067	0.2268	-0.00532
0.0814	-0.00102	0.2443	-0.00607
0.0932	-0.00127	0.2617	-0.00682
0.1047	-0.00132	0.2792	-0.00766

Yaw is an important way for underwater robot to extend one-dimensional motion into two-dimensional motion. Similarly, we designed a set of hydrodynamic simulations, as shown in Table 3. The table lists the computing results of the damping in ASR yaw motion under the condition of different yaw angular velocity in ANSYS. The hydrodynamic damping coefficients of yaw motion obtained by regression analysis of the above computing results.

The damping coefficients are often assumed to be linear based on the assumption of small disturbances. The relationship between the hydrodynamic damping of the robot and the yaw angular velocity without disturbances was identified as follows:

$$F_N = -0.0061r - 0.0771r^2 \tag{6}$$

From the identification formula and the regression analysis, we concluded that the damping of yaw motion was linearly related to the quadratic angular velocity and the first order angular velocity.

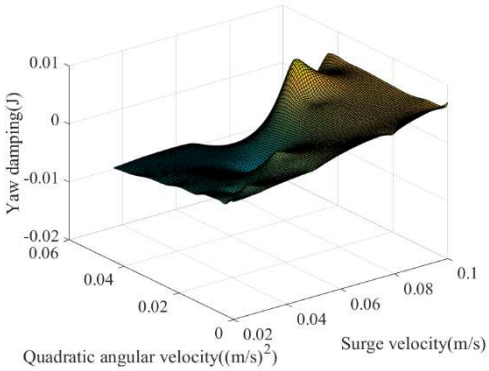

Fig. 8 The relationship curve between the damping torque of yaw motion and the quadratic angular velocity and the disturbance velocity (surge velocity)

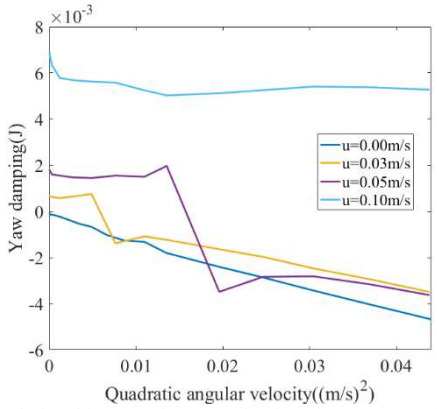

Fig. 9 The relationship curve between the damping torque and the quadratic velocity of the robot under different surge velocity as disturbance.

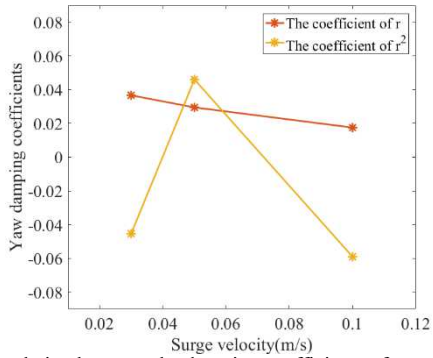

Fig. 10 The relation between the damping coefficients of yaw motion and the disturbance velocity in surge direction.

Furthermore, we designed the hydrodynamic simulation when the velocity disturbance existed in the surge direction of the robot, as shown in Fig. 8. We can see that the relationship

between yaw damping torque and the above two velocities was very complex. Therefore, we decomposed Fig. 8 into Fig. 9 according to the disturbance velocity.

Fig. 9 showed the relationship curve between the damping torque and the quadratic angular velocity of the robot under different surge velocity as disturbance. The damping coefficients were constant without disturbance. With the increase of the disturbance, the relationship between the damping coefficients and the quadratic angular velocity was no longer linear.

In Fig. 10, the relationship between the damping coefficients and the disturbance velocity was obtained through regression analysis. It was shown that the change of the damping coefficients with the increase of the disturbance velocity was very complex.

As a result, in the actual operation of the robot, the dynamic model of robot is difficult to predict and the control algorithm is difficult to be effective under the complex or large hydrodynamic disturbance. These disturbances are inevitable. Therefore, the study of the hydrodynamic damping coefficients under the disturbance is of great significance for the robot to better resist disturbance and move in the complex water environment.

C. *Simulation based on identification model*

Based on the identification model and theoretical values model about mass matrix, we used MATLAB to simulate the movement process of the robot in the state of yaw motion as verification. The purpose was to get the relevant movement information, so as to compare with appropriate information in the experimental stage.

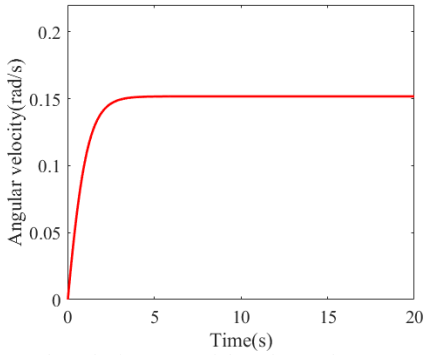

Fig. 11 The velocity curve of the robot under constant torque.

In the state of yaw motion, we added a constant torque on the z_b axis of the robot. Therefore, the robot first accelerated with a decreasing acceleration, and then moved at a constant velocity when it reached equilibrium state. The velocity curve of the robot under constant torque was shown in Fig. 11. We can see the smoothness and stability of the simulation results using the hydrodynamic damping coefficients getting above.

D. *Experiment and validation*

In order to verify the validity of the hydrodynamic coefficients of the model, we designed relevant experiments in a pool. The diagram of robot in the yaw motion was shown in Fig. 12.

Similar to the simulation method, we added a constant torque to the robot in the pool. The robot first accelerated and then moved at a constant velocity. Since the constant torque added to the robot in the experiment could not be accurately measured, we calibrated it accordingly. Then we compared the experimental and simulation results.

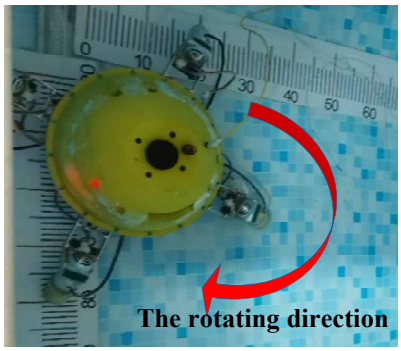

Fig. 12 The diagram of the robot in yaw motion.

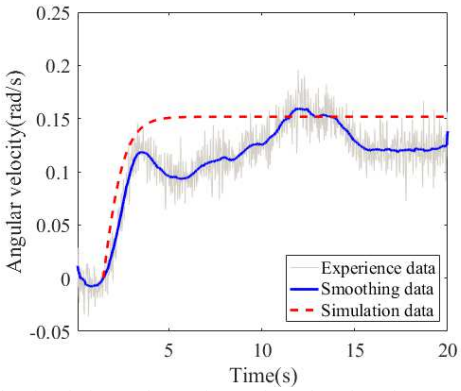

Fig. 13 The simulation and experimental results when the corrected torque is 0.0027N·m

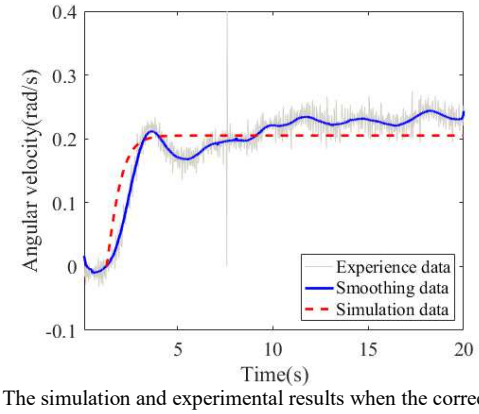

Fig. 14 The simulation and experimental results when the corrected torque is 0.0045N·m.

Considering the complexity of the underwater environment, the hydrodynamic characteristics of the robot changed with the generation of the disturbance flow, which was shown in the previous fluid calculation results. As shown in Fig. 13 and Fig. 14, the simulation results were in general fit with the experimental results. The simulation results basically reflected the movement trend of the robot under the action of

constant torque, and the qualitative velocity errors seemed to be small.

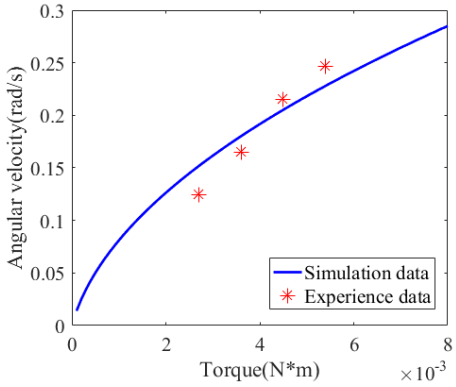

Fig. 15 The yaw motion velocity of the robot after reaching equilibrium (constant velocity motion) under different torques.

In addition, in order to better compare the errors between the simulation whose model established through CFD method and the actual experiment, we carried out relevant verification. The equilibrium velocity of the robot was calculated under different torques and compared with the experimental data. The velocity representing the experimental data was the average velocity of the robot after the first deceleration time. As shown in Fig. 15, we concluded that four groups of experimental data were distributed near the simulation data. This reflected the basic accuracy of the model. According to the data in the figure, we calculated the errors between the four groups of experimental data from left to right and the simulation is 0.027, 0.016, 0.011, 0.018rad/s, respectively. In the yaw motion of the robot, we concluded that the model established through fluid simulation can roughly simulated the movement of the robot in the actual environment.

IV. Conclusion

We set up the dynamics model of the robot through CFD simulation method. Then, the effectiveness of the robot dynamics model was verified by simulation and experimental analysis under the same setting. Due to the existence of disturbance flow, there were some errors between the simulation and the experiment results. This also verified that the hydrodynamic model of the robot was different under the disturbances. In addition, we also explored the hydrodynamic effects under different flow disturbances, which provided a reference for guiding the dynamic modeling and model-based control of the underwater robots.

Acknowledgment

This work was partly supported by National High Tech. Research and Development Program of China (No.2015AA043202), the National Natural Science Foundation of China (61773064, 61503028), the National Key Research and Development Program of China (No. 2017YFB1304401).

References

[1] H. Xing et al., "Design, modeling and experimental evaluation of a legged, multi-vectored water-jet composite driving mechanism for an amphibious spherical robot," *Microsystem Technologies-Micro-and Nanosystems-Information Storage and Processing Systems*, vol. 26, no. 2, pp. 475-487, February 2020.

[2] J. Guo, C. Li, and S. Guo, "Path Optimization Method for the Spherical Underwater Robot in Unknown Environment," *Journal of Bionic Engineering*, vol. 17, no. 5, pp. 944-958, September 2020.

[3] H. Xing et al., "Robust RGB-D Camera and IMU Fusion-based Cooperative and Relative Close-range Localization for Multiple Turtle-inspired Amphibious Spherical Robots," *Journal of Bionic Engineering*, vol. 16, no. 3, pp. 442-454, May 2019.

[4] X. Hou et al., "Improved Model Predictive-Based Underwater Trajectory Tracking Control for the Biomimetic Spherical Robot under Constraints," *Applied Sciences-Basel*, DOI：10.3390/mi11010071, 2020.

[5] L. Zheng et al., "Collaboration and Task Planning of Turtle-Inspired Multiple Amphibious Spherical Robots," *Micromachines*, vol. 11, no. 1, DOI:10.3390/mi11010071, January 2020.

[6] B. Liu, "Recent Advancements in Autonomous Robots and Their Technical Analysis," *Mathematical Problems in Engineering*, DOI: 10.1155/2021/663477, 2021.

[7] Z. Xu et al., "A comparison of functional control strategies for underwater vehicles: Theories, simulations and experiments," *Ocean Engineering*, vol. 215, DOI: 10.1016/j.oceaneng.2020.107822, 2020.

[8] R. Tian et al., "CFD based parameter tuning for motion control of robotic fish," *Bioinspiration & Biomimetics*, vol. 15, no. 2, DOI: 10.1088/1748-3190/ab6b6c, 2020.

[9] K. Alam, T. Ray, and S. Anavatti, "Design Optimization of an Unmanned Underwater Vehicle Using Low- and High-Fidelity Models," *IEEE Transactions on Systems Man Cybernetics-Systems*, vol. 47, no. 11, pp. 2794-2808, November 2017.

[10] H. Zheng, X. Wang, and Z. Xu, "Study on hydrodynamic performance and CFD simulation of AUV," DOI: 10.1109/ICInfA.2017.8078877, pp. 24-29, 2017.

[11] J. Yu et al., "Motion Control and Motion Coordination of Bionic Robotic Fish: A Review," *Journal of Bionic Engineering*, vol. 15, no. 4, pp. 579-598, July 2018.

[12] S. Guo et al., "Modeling and experimental evaluation of an improved amphibious robot with compact structure," *Robotics and Computer-Integrated Manufacturing*, vol. 51, no. 2, pp. 1339-1351, 2018.

[13] Y. He et al., "Underwater motion characteristics evaluation of multi amphibious spherical robots," *Microsystem Technologies-Micro-and Nanosystems-Information Storage and Processing Systems*, vol. 25, no. 2, pp. 499-508, February 2019.

[14] S. Gu and S. X. Guo, "Performance Evaluation of a Novel Propulsion System for the Spherical Underwater Robot (SURIII)," *Applied Sciences-Basel*, DOI：10.3390/app7111196, 2017.

[15] M. Porez, F. Boyer, and A. Ijspeert, "Improved Lighthill fish swimming model for bio-inspired robots: Modeling, computational aspects and experimental comparisons," *International Journal of Robotics Research*, vol. 33, no. 10, pp. 1322-1341, June 2014.

[16] S. Gu, S. Guo, and L. Zheng, "A highly stable and efficient spherical underwater robot with hybrid propulsion devices," *Autonomous Robots*, vol. 44, no. 5, pp. 759-771, May 2020.

[17] X. Hou et al., "Hydrodynamic Analysis-Based Modeling and Experimental Verification of a New Water-Jet Thruster for an Amphibious Spherical Robot," *Sensors*, vol. 19, no. 2, DOI: 10.3390/s19020259, 2019.

[18] R. Li et al., "A multi-body dynamics based numerical modelling tool for solving aquatic biomimetic problems," *Bioinspiration & Biomimetics*, vol. 13, no. 5, DOI: 10.1088/1748-3190/aacd60, 2018.

[19] H. Zhou et al., "Computational Hydrodynamics and Statistical Modeling on Biologically Inspired Undulating Robotic Fins: A Two-Dimensional Study," *Journal of Bionic Engineering*, vol. 7, no. 1, pp. 66-76, March 2010.

[20] R. Fernandez et al., "Motion Control of Underwater Mine Explorer Robot UX-1: Field Trials," *IEEE Access*, vol. 7, no. 2, pp. 99782-99803, DOI: 10.1109/ACCESS.2019.2930544, 2019.

[21] P. Jason, "Verification of a six-degree of freedom simulation model for the REMUS autonomous underwater vehicle," vol. 1, DOI: 10.1109/OCEANS.2001.968766 pp. 450-455 2011.

[22] M. Lamas and C. Rodriguez, "Hydrodynamics of Biomimetic Marine Propulsion and Trends in Computational Simulations," *Journal of Marine Science and Engineering*, DOI：10.3390/jmse8070479, 2020.